Hindawi
Journal of Applied Mathematics
Volume 2019, Article ID 8398035, 8 pages
https://doi.org/10.1155/2019/8398035

Research Article

A Smoothed l_0-Norm and l_1-Norm Regularization Algorithm for Computed Tomography

Jiehua Zhu and Xiezhang Li

Department of Mathematical Sciences, Georgia Southern University, Statesboro, GA 30460, USA

Correspondence should be addressed to Jiehua Zhu; jzhu@georgiasouthern.edu

Received 5 November 2018; Revised 5 April 2019; Accepted 13 May 2019; Published 2 June 2019

Academic Editor: Ying Hu

The nonmonotone alternating direction algorithm (NADA) was recently proposed for effectively solving a class of equality-constrained nonsmooth optimization problems and applied to the total variation minimization in image reconstruction, but the reconstructed images suffer from the artifacts. Though by the l_0-norm regularization the edge can be effectively retained, the problem is NP hard. The smoothed l_0-norm approximates the l_0-norm as a limit of smooth convex functions and provides a smooth measure of sparsity in applications. The smoothed l_0-norm regularization has been an attractive research topic in sparse image and signal recovery. In this paper, we present a combined smoothed l_0-norm and l_1-norm regularization algorithm using the NADA for image reconstruction in computed tomography. We resolve the computation challenge resulting from the smoothed l_0-norm minimization. The numerical experiments demonstrate that the proposed algorithm improves the quality of the reconstructed images with the same cost of CPU time and reduces the computation time significantly while maintaining the same image quality compared with the l_1-norm regularization in absence of the smoothed l_0-norm.

1. Introduction

Statistical and iterative reconstruction algorithms in computed tomography (CT) are widely applied since they yield more accurate results than analytic approaches for low-dose and limited-view reconstruction. These algorithms involve solving a linear system:

$$\Phi f + e = u, \tag{1}$$

where Φ is an $m \times n^2$ projection matrix, $f \in R^{n^2}$ represents a 2D $n \times n$ image to be reconstructed, e is an additive noise with $\|e\|_2 \leq \varepsilon$ for some known $\varepsilon > 0$, and $u \in R^m$ is the noisy projection data. For limited-view reconstruction, the underdetermined system ($m \ll n^2$) has infinitely many solutions. An optimal solution representing the original image as well as possible is sought by iteration methods.

The theory of compressed sensing [1–3] has recently shown that signals and images that have sparse representations in some orthonormal bases can be reconstructed at high quality from much less data than what the Nyquist sampling theory [4] requires. In many cases in tomography, images can be approximately modeled to be essentially piecewise constant so the gradients are sparse. With the gradient operator as a sparse transform, compressed sensing provides a novel framework for CT image reconstruction [1, 3, 5]. The l_0-norm of a vector, the number of its nonzero elements, is an appropriate measurement for the sparsity of a vector. So the l_0-norm regularization might be an approach for the reconstruction of an image with sparse gradient. However, the l_0-norm is a nonconvex function and the l_0-norm regularization problem is NP hard [6]. A pseudoinverse transform of the discrete gradient and the iterative hard thresholding algorithm are used to address the issues of the l_0-norm [7]. The smoothed l_0-norm (sl_0-norm) provides a smooth measure of sparsity and is applied in compressed sensing MRI imaging [8]. The sl_0-norm is used to find the jointly sparse representation via the low-resolution image [9]. sl_0-norm regularization model is proposed for sparse-view X-ray CT reconstruction [10]. Two new smoothed functions approximating the l_0-norm are proposed in the mechanism of reweighted regularization

[11, 12]. An edge-preserving image reconstruction method based on l_0-regularized gradient prior for limited-angle CT is investigated [13]. The local and global minimizers of l_0 gradient regularized model with box constraints for image restoration are discussed [14]. A new l_0 regularization and wavelet tight framelets to suppress the slope artifacts in the limited-angle X-ray CT reconstruction are addressed [15]. An image model based on l_0 and l_2 regularizations for the limited-angle CT is proposed, and the existence of a solution and a local convergence analysis under certain conditions are proved [16].

The l_1-norm regularization, known as total variation (TV) minimization [17], has been widely used in CT reconstruction. Under certain conditions, the l_1-norm minimization has a unique sparsest solution which is a good approximation to the original image [18]. However, the l_1-norm regularization provides less sparsity representation than the l_0-norm regularization and may lose some detailed features and contrast. In addition, the discrete gradient transformation ∇f does not satisfy the restricted isometry property required by the compressed sensing theory.

Researchers in this area have been seeking for other efficient and stable algorithms inspired by the compressed sensing theory, for example, solving an l_1-norm minimization with an l_2-norm constraint using the alternating direction method (ADM) [19, 20] and the nonmonotone alternating direction method (NADA) [21, 22]. Regularization including multiple norms is developed to address the drawbacks of the l_1-norm and l_0-norm. A combined l_1-norm and sl_0-norm regularization minimization with an l_2-norm constraint using SART algorithm and the gradient decent method is proposed for sparse-view CT image reconstruction in [23]. It is observed in the paper that the convergence is slow and the computation is time consuming because of the alternative minimization of the l_1-norm and sl_0-norm.

The purposes of this paper are multifold:

(i) Presenting a combined sl_0-norm and l_1-norm regularization algorithm for image reconstruction in CT: The proposed algorithm is unique in the following aspects: A new parameter is introduced to balance the sl_0-norm and l_1-norm terms; two-norm regularization is combined in one Lagrangian object function to be minimized

(ii) Adopting a newly developed alternating direction method NADA to efficiently solve minimization

(iii) Resolving the computation challenge problem caused from the sl_0-norm minimization

The numerical experiments demonstrate that the proposed algorithm improves the quality of the recovered images for the same cost of CPU time and reduces the computation time significantly while maintaining the same image quality compared with the l_1-norm regularization in absence of the sl_0-norm.

The rest of the paper is organized as follows. Section 2 includes the background and notations. In Section 3, a combined sl_0-norm and l_1-norm regularization algorithm with the NADA is developed. Numerical experiments with the Shepp-Logan phantom and a cardiac image are presented in Section 4. Finally, Section 5 concludes the paper by discussions and conclusions.

2. Background and Notations

The TV minimization of an image f for solving system (1) is mathematically represented as [17]

$$\begin{aligned} \min \quad & \|f\|_{TV} \\ \text{subject to} \quad & \Phi f + e = u, \end{aligned} \tag{2}$$

where the total variation $\|f\|_{TV}$ is the l_1-norm of the magnitude of the discrete gradients:

$$\|f\|_{TV} = \|\nabla f\|_1 = \sum_{i,j} \sqrt{\left(f_{i+1,j} - f_{i,j}\right)^2 + \left(f_{i,j+1} - f_{i,j}\right)^2}. \tag{3}$$

Then a 2D image f with sparse gradients and noisy measurements in CT can be reconstructed by solving the following l_1-norm minimization with an l_2-norm constraint:

$$\begin{aligned} \min_f \quad & \|\nabla f\|_1 \\ \text{subject to} \quad & \|\Phi f - u\|_2 \le \varepsilon, \end{aligned} \tag{4}$$

which can be implemented [24] by

$$\min_f \quad \left\{ \frac{\mu}{2} \|\Phi f - u\|_2^2 + \|\nabla f\|_1 \right\}. \tag{5}$$

Here $\mu > 0$ is a regularization parameter which controls the trade-off between sparsity of gradients and accuracy of approximation.

For convenience, we denote $D_p f$ as the forward difference of f at a pixel p in both horizontal and vertical directions; i.e.,

$$D_p f = D_{i,j} f = \left[f_{i+1,j} - f_{i,j}, f_{i,j+1} - f_{i,j} \right]^T \in R^2, \quad \text{for } p = (i-1)n + j. \tag{6}$$

Then $\|\nabla f\|_1 = \sum_{p=1}^{n^2} \|D_p f\|_2$ and minimization (5) is rewritten as

$$\min_f \quad \left\{ \frac{\mu}{2} \|\Phi f - u\|_2^2 + \sum_{p=1}^{n^2} \|D_p f\|_2 \right\}. \tag{7}$$

With the Lagrangian function [19, 20]

$$\begin{aligned} & L(f, v, \lambda) \\ & = \frac{\mu}{2} \|\Phi f - u\|_2^2 \\ & \quad + \sum_{p=1}^{n^2} \left\{ \|v_p\|_2 - \lambda_p^T \left(D_p f - v_p\right) + \frac{\beta}{2} \|D_p f - v_p\|_2^2 \right\}, \end{aligned} \tag{8}$$

minimization (7) is converted to

$$\min_f \quad L(f, v, \lambda), \tag{9}$$

which can be solved by the ADM [19–22]. The ADM is a variant of the classic augmented Lagrangian method for optimization. It has been applied to solve different types of l_1-minimization problems for sparse solution recovery. The kth step of the ADM for solving (9) involves the procedures

$$f^{k+1} = \arg\min_f L\left(f, v^k, \lambda^k\right); \tag{10}$$

$$v^{k+1} = \arg\min_v L\left(f^{k+1}, v, \lambda^k\right); \tag{11}$$

$$\lambda^{k+1} = \lambda^k + \beta\left(Df^{k+1} - v^{k+1}\right). \tag{12}$$

Minimization (10) and minimization (11) can be successfully solved using the framework of the NADA with a nonmonotone line search scheme recently developed in [21, 22]. The idea is outlined as follows.

(i) Choose a direction $d^k = -(\partial/\partial f)L(f^k, v^k, \lambda^k)$.

(ii) Select a step size s_k uniformly bounded above such that $L(f^k + s_k d^k, v^k, \lambda^k) \le C_k - s_k\delta\|d^k\|_2^2$, for $0 < \delta < 1$.

(iii) Set $f^{k+1} = f^k + s_k d^k$.

(iv) Compute C_{k+1} such that $L(f^{k+1}, v^k, \lambda^k) \le C_{k+1} \le C_k$.

Combined with the solution of (11), the sequence $\{L(f^k, v^k, \lambda^k)\}$ is bounded above by a monotonically nonincreasing sequence $\{C_k\}$ though $\{L(f^k, v^k, \lambda^k)\}$ itself is not decreasing. The advantage of the NADA lies in the fact that $L(f, v, \lambda)$ is not required to be differentiable while reducing the computation complexity and improving the efficiency. The convergence analysis of the NADA for solving a general model including minimization (11) can be found in [21].

The sl_0-norm approximates the l_0-norm by a smooth function [8]. The sl_0-norm of a vector $x \in R^{n^2}$, denoted by $\|x\|_{s0}$, is defined as

$$\|x\|_{s0} = n^2 - \sum_{j=1}^{n^2} \lim_{\sigma\longrightarrow 0} \exp\left(\frac{-x_j^2}{2\sigma^2}\right). \tag{13}$$

It is easy to see that $\|x\|_{s0} = \|x\|_0$.

A new approach for solving a more general minimization than the regularization minimization in [23] is proposed in the next section.

3. sl_0-Norm and l_1-Norm Regularization Algorithm

In this section we present sl_0-norm and l_1-norm regularization algorithm for CT reconstruction using the NADA. Consider the following constrained minimization problem for image reconstruction in CT:

$$\begin{aligned} \min_f \quad & \{\|\nabla f\|_1 + \alpha\|\nabla f\|_{s0}\} \\ \text{subject to} \quad & \|\Phi f - u\|_2^2 \le \varepsilon, \end{aligned} \tag{14}$$

where the parameter α is used to balance the two terms of the minimization. While the l_1-norm is used for the approximation accuracy, the sl_0-norm is introduced in consideration of the sparsity of gradients. It is remarked that minimization (14) is an extension of minimization (4) ($\alpha = 0$) and the minimization ($\alpha = 1$) in [23].

3.1. New Approach. The term $\|\nabla f\|_{s0}$ in (14) can be approximated by a smooth function

$$\begin{aligned} s_\sigma(\nabla f) &:= n^2 - \sum_{p=1}^{n^2} \exp\left(\frac{-\left|(\nabla f)_p\right|^2}{2\sigma^2}\right) \\ &= n^2 - \sum_{p=1}^{n^2} \exp\left(\frac{-\left\|D_p f\right\|_2^2}{2\sigma^2}\right) \end{aligned} \tag{15}$$

for a small positive parameter σ. So minimization (14) can be approximately obtained by solving

$$\begin{aligned} \min_f \quad & \{\|\nabla f\|_1 + \alpha s_\sigma(\nabla f)\} \\ \text{subject to} \quad & \|\Phi f - u\|_2^2 \le \varepsilon, \\ & \text{small } \sigma > 0. \end{aligned} \tag{16}$$

To deal with the constraint $\|\Phi f - u\|_2^2 \le \varepsilon$ in (16), we rewrite (16) with a positive parameter μ as

$$\begin{aligned} \min_f \quad & \left\{\frac{\mu}{2}\|\Phi f - u\|_2^2 + \|\nabla f\|_1 + \alpha s_\sigma(\nabla f)\right\}, \\ & \text{for small } \sigma > 0, \end{aligned} \tag{17}$$

or

$$\begin{aligned} \min_f \quad & \left\{\frac{\mu}{2}\|\Phi f - u\|_2^2 + \sum_{p=1}^{n^2}\|v_p\|_2 + \alpha s_\sigma\left(\|v_p\|_2\right)\right\}, \\ & \text{for small } \sigma > 0, \\ \text{subject to} \quad & D_p f = v_p, \quad 1 \le p \le n^2. \end{aligned} \tag{18}$$

Using a positive parameter β and Lagrange vectors $\lambda_p \in R^2$, $1 \le p \le n^2$, we define a Lagrangian function

$$\begin{aligned} L_\alpha(f, v, \lambda) = \frac{\mu}{2}\|\Phi f - u\|_2^2 + \sum_{p=1}^{n^2}\Big\{&\|v_p\|_2 \\ &- \lambda_p^T\left(D_p f - v_p\right) + \frac{\beta}{2}\left\|D_p f - v_p\right\|_2^2 \\ &+ \alpha s_\sigma\left(\|v_p\|_2\right)\Big\}. \end{aligned} \tag{19}$$

Finally, minimization (18) is converted to the following minimization:

$$\min_f \quad L_\alpha(f, v, \lambda). \tag{20}$$

It is obvious that $L_\alpha(f, v, \lambda)$ is an extension of $L(f, v, \lambda)$ in (8). Consequently the NADA is adopted to solve minimization

(20). The kth iteration for solving (20) includes the following steps:

$$f^{k+1} = \arg\min_{f} L_\alpha\left(f, v^k, \lambda^k\right), \tag{21}$$

$$v^{k+1} = \arg\min_{v} L_\alpha\left(f^{k+1}, v, \lambda^k\right), \tag{22}$$

$$\lambda^{k+1} = \arg\min_{\lambda} L_\alpha\left(f^{k+1}, v^{k+1}, \lambda\right). \tag{23}$$

It is noted that the objective function $L_\alpha(f, v, \lambda)$ in (19) has an extra term $\alpha s_\sigma(\|v_p\|)$, depending only on the vector v, compared with $L(f, v, \lambda)$ in (8). So the methods for the calculation of f^{k+1} in (10) and λ^{k+1} in (12) can be applied to the calculation of f^{k+1} in (21) and λ^{k+1} in (23). For example, in (23), $\lambda^{k+1} = \lambda^k + \beta(Df^{k+1} - v^{k+1})$. However, finding v^{k+1} in (22) is a challenging problem.

3.2. Calculation of v_p^{k+1}. In this subsection we address how to calculate v_p^{k+1} in (22) for $1 \le p \le n^2$. Actually, for each p, we need to solve for v_p from the following equation:

$$\frac{\partial L_\alpha}{\partial v_p} = \frac{v_p}{\|v_p\|_2} + \lambda_p - \beta D_p f + \beta v_p + \frac{\alpha v_p}{\sigma^2}\exp\left(\frac{-\|v_p\|_2^2}{2\sigma^2}\right) = 0. \tag{24}$$

It follows from (24) that

$$v_p\left[1 + \frac{1}{\beta\|v_p\|_2} + \frac{\alpha}{\beta\sigma^2}\exp\left(\frac{-\|v_p\|_2^2}{2\sigma^2}\right)\right] = D_p f - \frac{\lambda_p}{\beta}. \tag{25}$$

If $\|v_p\|_2$ is calculated then

$$v_p = \frac{\|v_p\|_2\left(D_p f - \lambda_p/\beta\right)}{\left\|D_p f - \lambda_p/\beta\right\|_2}. \tag{26}$$

Thus, it suffices to determine $\|v_p\|_2$ from the following equation:

$$\|v_p\|_2\left[1 + \frac{\alpha}{\beta\sigma^2}\exp\left(\frac{-\|v_p\|_2^2}{2\sigma^2}\right)\right] = \left\|D_p f - \frac{\lambda_p}{\beta}\right\|_2 - \frac{1}{\beta}. \tag{27}$$

Denote $c = \|D_p f - \lambda_p/\beta\|_2 - 1/\beta$. If $c \le 0$ we set $v_p = 0$. If $c > 0$, it follows from (27) that $\|v_p\|_2$ is a positive real solution of the equation

$$h(z) \coloneqq z + \frac{\alpha z}{\beta\sigma^2}\exp\left(\frac{-z^2}{2\sigma^2}\right) - c = 0. \tag{28}$$

It is obvious that there is a positive zero z of $h(z)$ between 0 and c and $z \longrightarrow c$ as $\sigma \longrightarrow 0$.

Equation (28) can be rewritten as

$$\exp\left(\frac{-z^2}{2\sigma^2}\right) = \frac{\beta\sigma^2(c - z)}{\alpha z} \quad \text{or} \quad \frac{z^2}{2\sigma^2} = \ln\frac{\alpha z}{\beta\sigma^2(c - z)}. \tag{29}$$

By substituting $z = \sqrt{w}$, the above equation becomes

$$s(w) \coloneqq w - 2\sigma^2\left(\ln\frac{\alpha\sqrt{w}}{\beta\sigma^2\left(c - \sqrt{w}\right)}\right) = 0, \quad \text{on } \left(0, c^2\right). \tag{30}$$

Thus, we have shown the following lemma.

Lemma 1. *Let $h(z)$ and $s(w)$ be given in (28) and (30), respectively. Then w is a zero of $s(w)$ on $(0, c^2)$ if and only if $z = \sqrt{w}$ is a zero of $h(z)$ on $(0, c)$.*

Before we develop a procedure to calculate a positive root of $s(w) = 0$, we will list some properties of $s(w)$ below.

It is known that

$$s'(w) = 1 - \frac{\sigma^2 c}{w\left(c - \sqrt{w}\right)} = \frac{-w\sqrt{w} + cw - \sigma^2 c}{w\left(c - \sqrt{w}\right)}. \tag{31}$$

With $z = \sqrt{w}$, the sign of $s'(w)$ on $(0, c^2)$ is the same as that of the function

$$q(z) \coloneqq -z^3 + cz^2 - \sigma^2 c \tag{32}$$

on $(0, c)$. By calculus, it is easy to see that $q(z)$ is increasing on $(0, (2/3)c)$ and decreasing on $((2/3)c, c)$ since $q'(z) = -z(3z - 2c)$. Thus, $q(z)$ achieves a local maximum $(4/27)c^3 - \sigma^2 c$ at $z = (2/3)c$. Therefore, if $(4/27)c^3 - \sigma^2 c > 0$ (or $\sigma < (2/3\sqrt{3})c$) then the equation $q(z) = 0$ has two positive roots z_1, z_2 with $z_1 < z_2$. It follows that $q(z) < 0$ on $(0, z_1) \cup (z_2, c)$ and $q(z) > 0$ on (z_1, z_2). On the other hand, if $\sigma > (2/3\sqrt{3})c$, then $q(z) < 0$ on $(0, c)$. We have the following monotonicity of $s(w)$.

Property 2. If $\sigma < (2/3\sqrt{3})c$ then $s(w)$ is increasing on (z_1^2, z_2^2) and decreasing on $(0, z_1^2)$ and (z_2^2, c^2), where z_1 and z_2 are two positive zeros of $q(z)$. If $\sigma \ge (2/3\sqrt{3})c$ then $s(w)$ is always decreasing on $(0, c^2)$.

The second derivative

$$s''(w) = \frac{\sigma^2 c}{w^2\left(c - \sqrt{w}\right)^2}\left(c - \frac{3}{2}\sqrt{w}\right) \tag{33}$$

indicates the following features of $s(w)$.

Property 3. $s''(w) > 0$ on $(0, (4/9)c^2)$ and $s''(w) < 0$ on $((4/9)c^2, c^2)$. The graph of $s(w)$ has an inflection point $P((4/9)c^2,\ (4/9)c^2 - 2\sigma^2\ln(2\alpha/\beta\sigma^2))$. The function $s(w)$ achieves a local minimum value at $w = z_1^2$ and a local maximum value at $w = z_2^2$. In addition, we have $\lim_{w\longrightarrow 0+} s(w) = \infty$ and $\lim_{w\longrightarrow c^2-} s(w) = -\infty$.

input $\Phi, u, \alpha, \varepsilon$
initialize $\beta, \mu, f^0, v^0, \lambda^0, maxit, \sigma, \delta, ratio, tol$
while $k < maxit$
1. update $f^{k+1} = \arg\min_f L_\alpha(f, v^k, \lambda^k)$ by the NADA
    1.1. decent direction $d^k = -(\partial/\partial f)L_\alpha(f^k, v^k, \lambda^k)$
    1.2. step size s_k such that $L_\alpha(f^k + s_k d^k, v^k, \lambda^k) \le C_k - s_k \delta \|d^k\|_2^2$
    1.3. update $f^{k+1} = f^k + s_k d^k$
    1.4. compute C_{k+1} such that $L_\alpha(f^{k+1}, v^k, \lambda^k) \le C_{k+1} \le C_k$
2. update $v^{k+1} = \arg\min_v L_\alpha(f^{k+1}, v, \lambda^k)$
    for $p = 1$ to n^2
    2.1. set $c = \|D_p f^{k+1} - \lambda_p^k/\beta\|_2 - 1/\beta$
    2.2. if $c \le 0$ then
        $v_p^{k+1} = 0$
    else
        select an initial guess w_0 from Theorem 4
        find a zero w of $s(w)$ in (30) by Newton's iterations
        $$v_p^{k+1} = \frac{\sqrt{w}(D_p f^{k+1} - \lambda_p^k/\beta)}{\|D_p f^{k+1} - \lambda_p^k/\beta\|_2}$$
    end if
    end for
3. update $\lambda^{k+1} = \lambda^k + \beta(Df^{k+1} - v^{k+1})$
4. if $error < tol$ then exit
5. update $\sigma = \sigma \times ratio$; $k = k + 1$
end while
output f^{k+1} and $error$

Algorithm 1: Calculation process of $sl_0 + l_1$ regularization algorithm (sl_0-norm and l_1-norm regularization algorithm).

Finally, we can determine the locations of zeros of $s(w)$ by convergent Newton's iterations.

Theorem 4. *Let $s(w)$ and $q(z)$ be, respectively, given in (30) and (32), where $z = \sqrt{w}$. Let z_2 be a larger positive root of $q(z)$ on $(0, c)$ for $\sigma < (2/3\sqrt{3})c$. Then a positive root of $s(w) = 0$ on $(0, c^2)$ can be calculated by Newton's method. The convergence of Newton's method is guaranteed if an initial guess w_0 is selected as follows.*

Case 1. (i) $\sigma < (2/3\sqrt{3})c$, $s(z_2^2) > 0$ or (ii) $\sigma \ge (2/3\sqrt{3})c$, $(2/9)c^2 - \sigma^2 \ln(2\alpha/\beta\sigma^2) > 0$.

Choose $w_0 < c^2$ and near c^2 with $s(w_0) < 0$.

Case 2. (i) $\sigma < (2/3\sqrt{3})c$, $s(z_2^2) < 0$ or (ii) $\sigma \ge (2/3\sqrt{3})c$, $(2/9)c^2 - \sigma^2 \ln(2\alpha/\beta\sigma^2) < 0$.

Choose $w_0 = (\beta\sigma^2 c/(\alpha + \beta\sigma^2))^2$.

Proof. We identify an interval containing a positive root of $s(w) = 0$ on which $s'(w)$ and $s''(w)$ do not change signs for each subcase. Then the convergence of Newton's method with an initial guess above is guaranteed.

Case 1. For subcase (i), there is a positive solution of $s(w) = 0$ on (z_2^2, c^2) on which both $s'(w)$ and $s''(w)$ are negative. For subcase (ii), the inflection point P of the graph of $s(w)$ is on the upper half plane. So a positive zero is on $((4/9)c^2, c^2)$ on which both $s'(w)$ and $s''(w)$ are negative. So one should choose $w_0 < c^2$ and near c^2 with $s(w_0) < 0$ for the convergence of Newton's method.

Case 2. For subcase (i), there is a positive solution of $s(w) = 0$ on $(0, z_1^2)$ on which $s'(w) < 0$ and $s''(w) > 0$. For subcase (ii), the inflection point P is on the lower half plane. So a positive zero is on $(0, (4/9)c^2)$ on which $s'(w) < 0$ and $s''(w) > 0$. One could choose $w_0 = (\beta\sigma^2 c/(\alpha + \beta\sigma^2))^2$ for the convergence of Newton iteration since $\beta\sigma^2 c/(\alpha + \beta\sigma^2)$ is a lower bound of positive solutions of $h(z) = 0$ on $(0, c)$ in (28). □

Thus, $\|v_p^{k+1}\|_2$, $1 \le p \le n^2$, can be calculated from Lemma 1 and Theorem 4. Then v^{k+1} in (26) can be obtained.

3.3. Algorithm. Based on the above discussion, the calculation process of the proposed $sl_0 + l_1$ regularization algorithm is summarized in Algorithm 1.

4. Numerical Experiments and Results

In this section, the proposed combined sl_0-norm and l_1-norm regularization is compared with the regularization without sl_0-norm for its performance. Both regularization algorithms are implemented using the NADA. The MATLAB code is developed based on the software package TVAL3 [22], and the numerical experiments are conducted on an Intel Core i7 3.40 GHz PC. The 2D Shepp-Logan phantom and a cardiac image [25] of size 128×128 are tested. In each test, a random

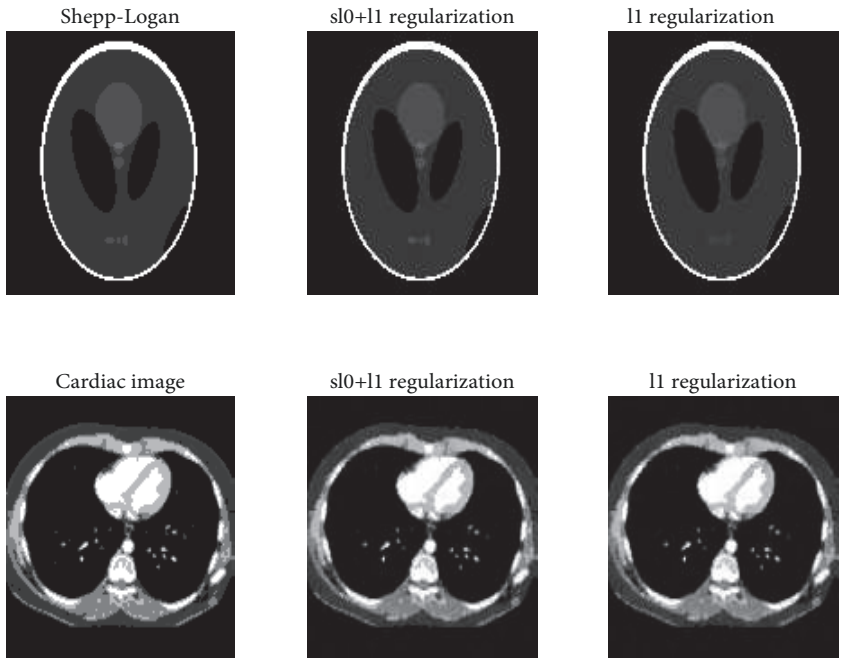

Figure 1: Original and reconstructed images. First row: Shepp-Logan phantom after 150 iterations. Second row: cardiac image after 80 iterations.

Table 1: Comparison of two algorithms after same number of iterations.

(a)

Shepp-Logan Phantom, after 70 iterations						
	Time(s)	Error	RMSE	NRMSD	NMAD	SSIM
l_1 regularization	9.5	0.121	0.030	0.031	0.124	0.826
$sl_0 + l_1$ regularization	6.3	0.067	0.016	0.017	0.068	0.912

(b)

Cardiac Image, after 50 iterations						
	Time(s)	Error	RMSE	NRMSD	NMAD	SSIM
l_1 regularization	5.1	0.131	0.047	0.033	0.152	0.696
$sl_0 + l_1$ regularization	4.9	0.116	0.042	0.029	0.131	0.735

matrix $\Phi \in R^{m\times n^2}$ ($m \approx 0.3n^2$) is used to create the same system $u = \Phi f + e$ for two regularization algorithms, where the noise $e = 0.02*\text{mean}(\Phi f)*\text{randn}(m)$. The parameters are taken as $\alpha = 1$, $\beta = 2^3$, $\mu = 2^5$ for the Shepp-Logan phantom and $\alpha = 1$, $\beta = 2^4$, $\mu = 2^7$ for the cardiac image, respectively. The values of the parameter σ in the sl_0-norm are decreasing at a ratio of 0.9 with a starting value $\sigma_0 = 0.1$.

Experiments are conducted to compare the reconstruction by the two algorithms after the same number of iterations. The original/reconstructed Shepp-Logan phantom images and the original/reconstructed cardiac images after same numbers of iterations are shown in Figure 1. The reconstructed images show that the proposed $sl_0 + l_1$-norm regularization produces better images while taking about 75% of the CPU time.

The quality of images is evaluated using the relative error $\|f - f_{recon}\|_F / \|f\|_F$ of the reconstructed image f_{recon} in Frobenius norm. The root-mean-square error (RMSE), the normalized root-mean-square deviation (NRMSD), the normalized mean absolute deviation (NMAD), and the structural similarity index (SSIM) are also measured to reflect different aspects of the quality of the recovered images. RMSE evaluates the reconstruction quality on a pixel-by-pixel basis. NRMSD emphasizes large errors in a few pixels of the recovered image. NMAD focuses on small errors in the recovered image. SSIM compares the quality of the images using the original phantom image as a reference. A greater value of an SSIM indicates the better image quality. The experimental results from 100 tests are summarized in Table 1. The data in Table 1 indicates that the proposed $sl_0 + l_1$-norm regularization provides a better accuracy after the same iteration number.

Experiments are also conducted to compare iteration numbers and CPU time by the two algorithms when the same

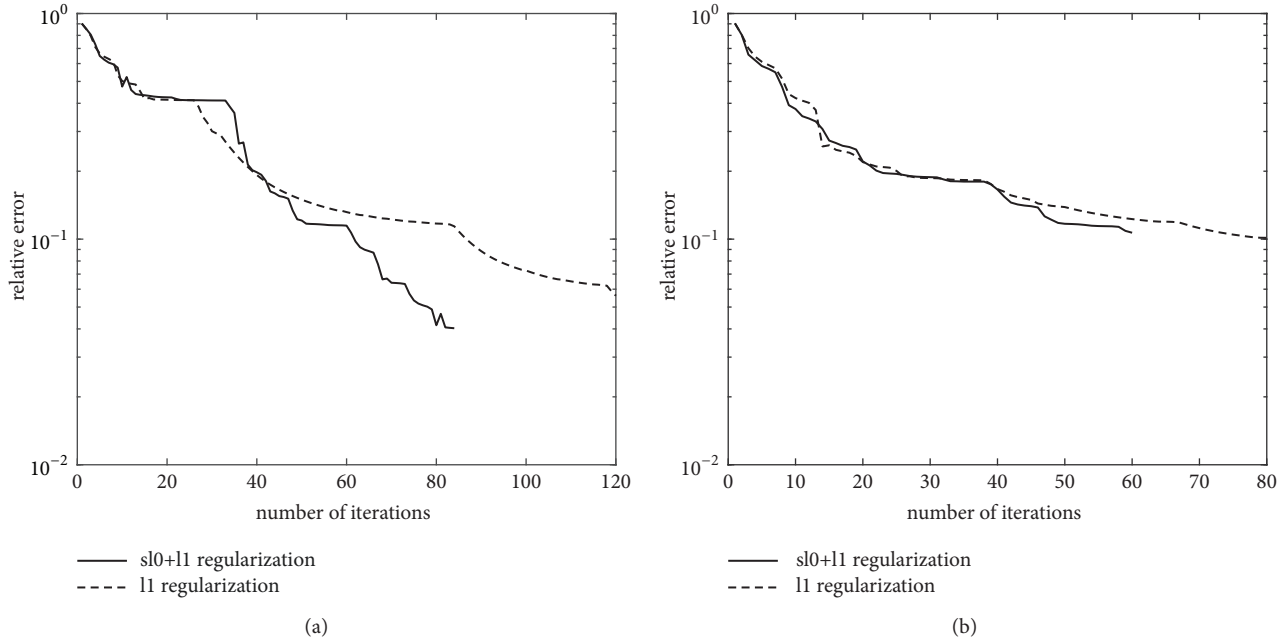

Figure 2: Relative error vs. iteration number in reconstruction by two algorithms to achieve the same tolerance of relative error 0.05. (a) Shepp-Logan phantom; (b) cardiac image.

Table 2: Comparison of two algorithms with the same tolerance of relative error 0.05.

Phantom	l_1 Regularization		$sl_0 + l_1$ Regularization		CPU Time Saved
	No. Iter.	Time(s)	No. Iter.	Time(s)	
Shepp-Logan	129	17.4	86	7.4	58%
Cardiac	194	24.9	178	19.4	22%

relative error is achieved and thus the image quality is same. The tolerance of the relative error to terminate the iteration is selected as 0.05. The average iteration numbers and CPU time from 100 tests of the $sl_0 + l_1$-norm regularization and l_1-norm only regularization are listed in Table 2. The comparison indicates that the CPU time is significantly reduced in the proposed algorithm while producing the same image quality. The graph of relative errors vs. the number of iterations for the two algorithms, shown in Figure 2, indicates that the $sl_0 + l_1$-norm regularization requires less iterations to achieve the same accuracy.

Both types of the numerical experiments demonstrate that the proposed $sl_0 + l_1$-norm regularization is superior to the regular l_1-norm regularization minimization.

5. Discussions and Conclusions

The application of the sl_0-norm in CT reconstruction has become one of active research topics recently. A combined sl_0-norm and l_1-norm regularization algorithm is proposed in this paper. The sl_0-norm of a vector x is the limit of a smooth convex function $s_\sigma(x)$. In iterations of the proposed algorithm, the parameter σ is getting smaller and closer to zero. The smooth function $s_\sigma(\nabla f)$ in the objective function $L_\alpha(f, v, \lambda)$ approaches $\|\nabla f\|_0$, and the sparsity of the recovered image is fulfilled quickly. So the proposed algorithm improves the quality of the reconstructed images and the efficiency in terms of the iteration number and CPU time even with the extra computation from the added sl_0-norm term. The numerical results demonstrate that the proposed algorithm improves the l_1-norm regularization with the NADA in reducing the computation time significantly. The effects of the weight parameter α of the sl_0-norm and the sl_0-norm parameter σ are also tested. From our experiments, the parameter α from 0.5 to 2 and the initial value σ_0 from 0.05 to 0.9 almost do not affect the efficiency of the algorithm. The decreasing ratio of parameter σ between 0.8 and 0.95 is a good choice, but a ratio smaller than 0.7 is not recommended.

There are some aspects to be further investigated. It is a challenging problem to select good values of other parameters such as β and μ in the Lagrangian function $L_\alpha(f, v, \lambda)$. The impact of these parameters on the performance of the algorithm will be further investigated.

Data Availability

The MATLAB numerical data used to support the findings of this study are available from the corresponding author upon request.

Conflicts of Interest

The authors declare that they have no conflicts of interest.

References

[1] E. J. Candes, J. Romberg, and T. Tao, "Robust uncertainty principle: exact signal reconstruction from highly incomplete frequency information," *IEEE Transactions on Information Theory*, vol. 52, no. 2, pp. 489–509, 2006.

[2] E. Candes and M. Wakin, "An introduction to compressive sampling," *IEEE Signal Processing Magazine*, vol. 25, no. 2, pp. 21–30, 2008.

[3] D. L. Donoho, "Compressed sensing," *IEEE Transactions on Information Theory*, vol. 52, no. 4, pp. 1289–1306, 2006.

[4] C. E. Shannon, "Communication in the presence of noise," *Proceedings of the IEEE*, vol. 86, no. 2, pp. 447–457, 1998.

[5] E. J. Candes and T. Tao, "Decoding by linear programming," *IEEE Transactions on Information Theory*, vol. 51, no. 12, pp. 4203–4215, 2005.

[6] B. K. Natarajan, "Sparse approximate solutions to linear systems," *SIAM Journal on Computing*, vol. 24, no. 2, pp. 227–234, 1995.

[7] Y. Sun and J. Tao, "Image reconstruction from few views by ℓ_0-norm optimization," *Chinese Physics B*, vol. 23, no. 7, Article ID 078703, 2014.

[8] H. Mohimani, M. Babaie-Zadeh, and C. Jutten, "A fast approach for overcomplete sparse decomposition based on smoothed ℓ_0 norm," *IEEE Transactions on Signal Processing*, vol. 57, no. 1, pp. 289–301, 2009.

[9] M. Rostami and Z. Wang, "Image super-resolution based on sparsity prior via smooth ℓ_0 norm," in *Proceedings of the Symposium on Advanced Intelligent Systems*, Waterloo, Canada, December 2011.

[10] M. Li, C. Zhang, C. Peng et al., "Smoothed ℓ_0 norm regularization for sparse-view X-ray CT reconstruction," *BioMed Research International*, vol. 2016, Article ID 2180457, 12 pages, 2016.

[11] L. Wang, X. Yin, H. Yue, and J. Xing, "A regularized weighted smoothed l0-norm minimization method for underdetermined blind source separation," *Sensors*, vol. 18, no. 12, 2018.

[12] X. Yin, L. Wang, H. Yue, and J. Xiang, "A new non-convex regularized sparse reconstruction algorithm for compressed sensing magnetic resonance image recovery," *Progress in Electromagnetics Research C*, vol. 87, pp. 241–253, 2018.

[13] W. Yu, C. Wang, and M. Huang, "Edge-preserving reconstruction from sparse projections of limited-angle computed tomography using ℓ_0-regularized gradient prior," *Review of Scientific Instruments*, vol. 88, no. 4, Article ID 043703, 2017.

[14] X. Feng, C. Wu, and C. Zeng, "On the local and global minimizers of ℓ_0 gradient regularized model with box constraints for image restoration," *Inverse Problems*, vol. 34, no. 9, Article ID 095007, 2018.

[15] L. Zhang, L. Zeng, and Y. Guo, "l0 regularization based on a prior image incorporated non-local means for limited-angle X-ray CT reconstruction," *Journal of X-Ray Science and Technology*, vol. 26, no. 3, pp. 481–498, 2018.

[16] C. Wang, L. Zeng, W. Yu, and L. Xu, "Existence and convergence analysis of l0 and ℓ_2 regurizations for limited-angle CT reconstruction," *Inverse Problems and Imaging*, vol. 12, no. 3, pp. 545–572, 2018.

[17] E. J. Candes, M. B. Wakin, and S. P. Boyd, "Enhancing sparsity by reweighted l_1 minimization," *Journal of Fourier Analysis and Applications*, vol. 14, no. 5-6, pp. 877–905, 2008.

[18] H. Zhang, W. Yin, and L. Cheng, "Necessary and sufficient conditions of solution uniqueness in ℓ_1-norm minimization," *Journal of Optimization Theory and Applications*, vol. 164, no. 1, pp. 109–122, 2015.

[19] M. Tao and F. Yang, "Alternating direction algorithms for total variation deconvolution in image reconstruction," Optimization Online TR0918, Department of Mathematics, Nanjing University, 2009.

[20] J. Yang and Y. Zhang, "Alternating direction algorithms for ℓ_1-problems in compressive sensing," *SIAM Journal on Scientific Computing*, vol. 33, no. 1, pp. 250–278, 2011.

[21] C. Li, W. Yin, H. Jiang, and Y. Zhang, "An efficient augmented Lagrangian method with applications to total variation minimization," *Computational Optimization and Applications*, vol. 56, no. 3, pp. 507–530, 2013.

[22] C. Li, W. Yin, and Y. Zhang, "User's guide for TVAL3: TV minimization by augmented Lagrangian and alternating direction algorithms," CAAM Report, 2010.

[23] H. Qi, Z. Chen, J. Guo, and L. Zhou, "Sparse-view computed tomography image reconstruction via a combination of L1 and SL0 regularization," *Bio-Medical Materials and Engineering*, vol. 26, pp. S1389–S1398, 2015.

[24] S. S. Chen, D. L. Donoho, and M. A. Saunders, "Atomic decomposition by basis pursuit," *SIAM Journal on Scientific Computing*, vol. 20, no. 1, pp. 33–61, 1998.

[25] TEAM RADS, http://teamrads.com/.